Available online at www.sciencedirect.com

ScienceDirect

Proceedings of the Combustion Institute 37 (2019) 1733–1739

Proceedings of the Combustion Institute

www.elsevier.com/locate/proci

Laminar flame propagation in supercritical hydrogen/air and methane/air mixtures

Wenkai Liang*, Weiyu Li, Chung K. Law

Department of Mechanical and Aerospace Engineering, Princeton University, Princeton, NJ 08544, USA

Received 29 November 2017; accepted 7 June 2018
Available online 5 July 2018

Abstract

The propagation of laminar hydrogen/air and methane/air flames in supercritical conditions was computationally simulated for the planar flame configurations, incorporating descriptions of supercritical thermodynamics and transport as well as high-pressure chemical kinetics. The inaccuracies associated with the use of ideal gas assumptions for various components of the supercritical description were systematically assessed with progressively more complete formulation. Results show that, for hydrogen/air flames, the laminar flame speeds at high pressures increase due to the non-ideal equation of state (EoS), and is mainly due to the density modification of the initial mixture. Including the thermodynamic properties of heat capacity reduces the flame speed because of the correspondingly reduced adiabatic flame temperature. Transport properties were found to have small effect because of the inherent insensitivity of the laminar burning rate to variations in the transport properties. For methane/air flames, the use of recently reported high-pressure chemical kinetics considerably affects the laminar flame speed, even for the same flame temperature.

Keywords: Laminar flame speed; Hydrogen; Methane; Supercritical combustion

1. Introduction

Combustion under high-pressure conditions holds the potential for improved thermodynamic efficiency, enhanced power generation, and reduced emission of some pollutants. It underlies the technology of internal combustion engines such as the automotive engine, the gas turbine, and the rocket engine [1–3], for which the operating pressure can reach as high as hundreds of atmospheres [3]. At such high-pressure conditions, the fluid can be locally or even globally at the supercritical state, and as such is subjected to considerable real-fluid effects. Recognizing that studies of high-pressure combustion have frequently adopted ideal-gas approximations to describe the thermodynamics, transport and chemical kinetics components of the problem, it behoove us to assess the extent of inaccuracy embedded in such approximations.

Most previous investigations on supercritical and transcritical combustion have involved *diffusion flames* [4–8]. Specifically, Ribert et al. [4]

* Corresponding author.
E-mail address: wenkail@princeton.edu (W. Liang).

https://doi.org/10.1016/j.proci.2018.06.070

numerically investigated hydrogen/oxygen counterflow diffusion flames of general fluids by incorporating subcritical and supercritical thermodynamic and transport properties. Pons et al. [5] studied the effects of mass transfer in transcritical nonpremixed counterflow and identified the sharp density gradients under such conditions. Furthermore, the scaling laws of flame thickness, heat release rate and species profiles in hydrogen and hydrocarbon counterflow diffusion flames were assessed by numerical simulations in [6,7]. Recently, Juanós and Sirignano [8] evaluated different levels of assumptions of ideal and dilute gases for the high-pressure real fluid effects in methane/air and methane/water–air diffusion flames for methane hydrate applications.

Only limited studies, however, have been conducted on *premixed flames* at supercritical conditions. Notably, Candel et al. [9] experimentally investigated the flame stabilization mechanism at supercritical conditions; while the propagation of planar hydrogen/oxygen/nitrogen flames was numerically studied in [10], showing that non-idealities in the equation of state (EoS) and the transport fluxes have strong influence on the cold zone of the flame.

The present study aims to extend these previous worthy studies along several directions, for *premixed flame* propagation. First, recognizing that most previous investigations involved hydrogen flames, in the present study we shall also include methane flames, as methane not only is the simplest hydrocarbon, it is also relevant for high-pressure applications including rocket propulsion and methane-hydrate utilization [8]. Second, we shall systematically identify the effects of various aspects of non-ideality for laminar flame propagation at progressively more complete levels of formulation. Third, we shall incorporate recently developed high-pressure methane oxidation mechanisms in our simulation, thereby assess the influence of high-pressure chemistry on the flame response. It is noted that the importance of realistic description of chemistry is essential for such practical problems as flame stabilization and blowoff, and for such fundamental issues as the meaningful extraction of chemical kinetics from the experimental data of laminar flame speeds.

In light of the above motivations, the current work numerically investigates the real-fluid effect on the planar flame propagating at supercritical conditions. In the following, we shall first present the models of supercritical fluid properties and the numerical method. Then, the laminar flame speeds and burning fluxes of hydrogen/air and methane/air mixtures are assessed and the inaccuracies of these parameters due to the non-ideal thermodynamic and transport properties and high-pressure chemical kinetics are evaluated and discussed.

2. Numerical methods and real-fluid models

The planar flame simulation is performed by the PREMIX package [11] from the CHEMKIN code. For hydrogen, the recent kinetic model by Burke et al. [12] is used; while for methane, the GRI Mech 3.0 [13], the USC Mech 2.0 methane sub-model [14], the HP Mech methane sub-model [15] and the recently updated high-pressure methane sub-mechanism from Hashemi et al. [16] are adopted.

To account for the non-ideality of dense fluids, we use the Soave–Relic–Kong (SRK) EoS [17], whose accuracy is generally accepted for wide range of fluid states:

$$P = \frac{RT}{v-b} - \frac{a}{v(v+b)} \tag{1}$$

where P is the pressure, T the temperature, v the molar volume, R the gas constant, and a, b are two parameters which for multicomponent mixtures follow the mixing rules:

$$a = \sum_i \sum_j X_i X_j \sqrt{a_i a_j}\; b = \sum_i X_i b_i \tag{2}$$

for which a_i, b_i are the parameters of the $i$thth species, and X_i its mole fraction. For the major species, such as H_2, CH_4 and N_2, the individual parameters, a_i, b_i, are evaluated by the critical state conditions $T_{c,i}, P_{c,i}$ [17]. For other minor species, such as the H, OH and CH_3 radicals, these two parameters are estimated by the Lennard–Jones potentials with the formulation in [10]. Furthermore, for methane, these parameters for the NO_x species are neglected.

Following the SRK EoS, the specific enthalpy can be determined as the sum of the ideal specific enthalpy and the departure function:

$$h = h_{\text{ideal}} + \frac{1}{W}\left[RT(Z-1) + \frac{T\frac{da}{dT} - a}{b}\ln\frac{b+v}{v}\right] \tag{3}$$

where h_{ideal} is the specific enthalpy for the ideal gas, W the average molecular weight, and $Z = Pv/RT$. The specific enthalpy for each individual species, h_i, can be evaluated by this formula as well. We note in passing that the mixing rule for the enthalpy of multicomponent mixtures, $h = \sum_i Y_i h_i$, is not valid when considering real-fluid effects [8] because it neglects the interaction among different species, which is included in the departure function formulation. Consequently, the commonly used transformation for the convective term that $\frac{dh}{dx} - \sum_i h_i \frac{dY_i}{dx} = \sum_i Y_i \frac{dh_i}{dx} = c_P \frac{dT}{dx}$ is not valid for real fluids, and the energy equation based on the sensible enthalpy or temperature cannot be used in such situations. Consequently, in the present simulation the energy equation based on the total enthalpy is adopted.

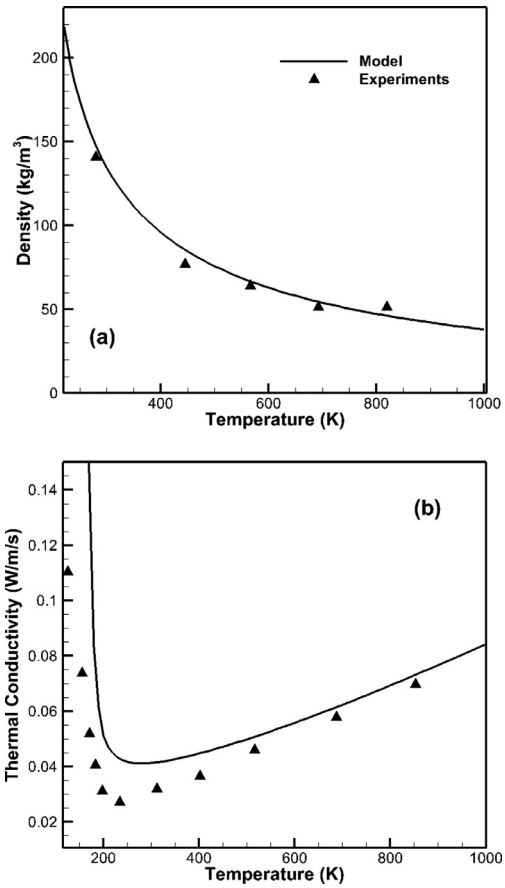

Fig. 1. Comparison of model and experimental data of (a) density and (b) thermal conductivity for oxygen at 100 atm.

For the transport properties, the real fluid models for both the thermal conductivity and mass diffusivity are incorporated. The thermal conductivity is evaluated from the correlation of Ely and Hanley [18]. Due to the small average molecular weight of hydrogen, this model would overpredict the flame speeds of rich hydrogen/air mixtures even at normal pressure. Thus, the modified mixing rule and conformal mapping are used for rich hydrogen/air mixtures to avoid such errors. For mass diffusion, the binary diffusion coefficients are corrected for the high-pressure conditions by the approach of Takahashi [19]. Furthermore, the mixture-averaged formulation is used. The predictions of density, heat capacity, thermal conductivity and mass diffusivity agree well with the experimental data as demonstrated in the literature [5–8,10]. To demonstrate the accuracy of these thermodynamic and transport models, the model predictions are compared with the experimental data from the NIST database [20] in Fig. 1. The results show that these models can accurately predict

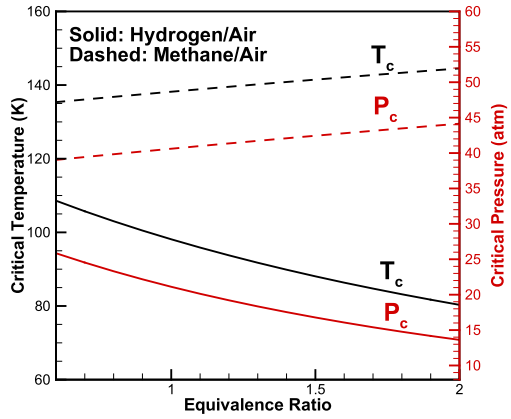

Fig. 2. Critical temperature and pressure for hydrogen/air and methane/air mixtures at various equivalence ratios.

the thermal and transport properties at supercritical conditions, although with small discrepancy at low-temperature conditions, below the room temperature.

In order to identify the inaccuracies due to each of the updated models, five different cases with progressively more real-fluid properties were designed. Specifically, Case 1 is the complete ideal-gas description serving as the starting, reference case for comparison. Cases 2-5 incorporate four real-fluid corrections: Case 2 replaces the ideal-gas law by the SRK EoS; Case 3 further incorporates the non-ideal enthalpy formulation in the energy equation; Case 4 adds the high-pressure thermal conductivity correction; and Case 5 adds the high-pressure mass diffusion model. Effects of high-pressure chemistry are then implemented.

3. Results and discussion

We start by analyzing the prototypical, adiabatic planar flames of hydrogen/air and methane/air mixtures propagating in the doubly infinite domain. Figure 2 shows the critical points (T_c and P_c) for these two mixtures calculated by using the SRK EoS as the inflection point in the P-v diagram. It is seen that the critical points of the hydrogen/air mixture are lower than those of methane, hence indicating that higher pressures are needed to induce supercritical effects for methane. In addition, the critical temperatures for both mixtures are always below the room temperature, so high critical pressure is the primary limitation in reaching the supercritical state. Moreover, for hydrogen/air, the critical point decreases with increasing equivalence ratio, while for methane/air the trend is the opposite. This is due to the relatively high critical point of methane ($T_c = 190$ K and $P_c = 46$ atm) and the relatively low critical point of hydrogen

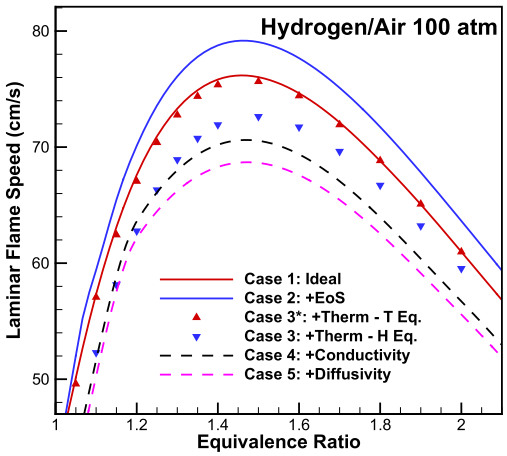

Fig. 3. Laminar flame speeds of hydrogen/air at 100 atm with different assumptions.

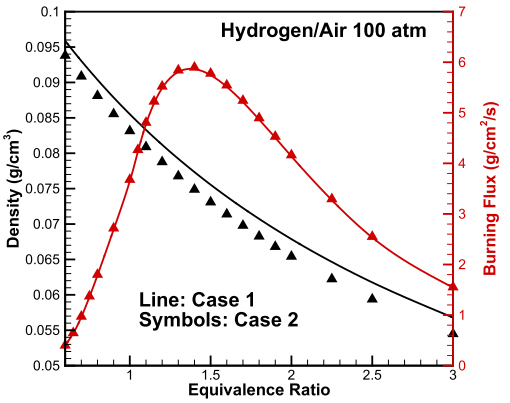

Fig. 4. Densities and burning fluxes of hydrogen/air at 100 atm for Cases 1 and 2.

($T_c = 33$ K and $P_c = 12$ atm), as compared to nitrogen ($T_c = 126$ K and $P_c = 33$ atm) and oxygen ($T_c = 154$ K and $P_c = 50$ atm).

The planar flames of hydrogen/air and methane/air mixtures considering the five test cases have been simulated from low to high pressures (1–100 atm). Since predictions of the five cases are almost identical for $P = 1$ atm, only the high-pressure results of 100 atm are presented.

3.1. Planar hydrogen/air flames

Figure 3 then shows the laminar flame speed of hydrogen/air mixtures at 100 atm with different assumptions (Cases 1–5). In addition, to quantify the error induced by using the temperature form of the energy equation, Case 3* is the case in which the thermodynamic properties are updated with the supercritical models but with the (incorrect) temperature equation instead of the proper enthalpy equation.

To quantify the effect of EoS, by comparing Cases 1 and 2 we find that using the SRK EoS results in higher flame speeds than those of the ideal gas. To explain this trend, the density of the initial mixtures of Cases 1 and 2 is presented in Fig. 4. Since the density of hydrogen is much smaller than that of air, its mixture density decreases with increasing equivalence ratio. The results then show that, by incorporating the SRK EoS, the density becomes lower than that of the ideal gas because the mixture behaves as a real fluid rather than an ideal gas at such high pressures. Further noting that the eigenvalue of the one-dimensional planar flame is the burning flux (i.e., the burning rate), $f = \rho S_L$, rather than the laminar flame speed S_L [21], where ρ is the unburned density, we have in addition plotted f in Fig. 4. It is then seen that the burning fluxes of Cases 1 and 2 are almost identical. This therefore indicates that the updated EoS does not change the eigenvalue of the flame propagation, and as such the increase of the laminar flame speed observed in Fig. 3 is primarily due to the decrease in the upstream density, as shown in Fig. 4, while the burning flux is minimally affected. This finding suggests that, for high-pressure flame speed measurements and comparisons, interpretation of the experimental and computational results of laminar flame speeds needs to recognize the density effect.

We next assess the effects of thermodynamic properties and the format of the energy equation by comparing Cases 2–3. Figure 3 shows that from Case 2 to Case 3, the laminar flame speed decreases. While this real-fluid thermodynamics effect is opposite to that of the EoS, at stoichiometric condition the laminar flame speed of Case 3 is still lower than Case 1 and Case 2, which is beyond the uncertainty of most flame speed measurements. The cause for this reduction is mainly the corresponding reduction of the adiabatic flame temperature, and through it the global reaction rate, as shown for Cases 1–3 in Fig. 5. To further elucidate this effect, we note that the adiabatic flame temperature can be approximately expressed as $T_{ad} = \Delta H / C_p$, where ΔH is the difference of enthalpy between the reactants and products and C_p is the heat capacity; the effect due to product dissociation is relatively small at such high pressures and as such not included in the assessment. For real fluids, C_p slightly increases; consequently this leads to the reduced T_{ad} as shown in Fig. 5 by comparing Case 2 and Case 3*. Furthermore, by using the enthalpy form of the equation, this effect further leads to even smaller flame speeds as shown in Fig. 3 by comparing Case 3* and Case 3.

We next examine the effect of transport properties on the laminar flame speed. Case 3 to Case 5 in Fig. 3 show that there is little effect on the flame speed when either the heat conductivity or the mass diffusivity is modified with the real-fluid mod-

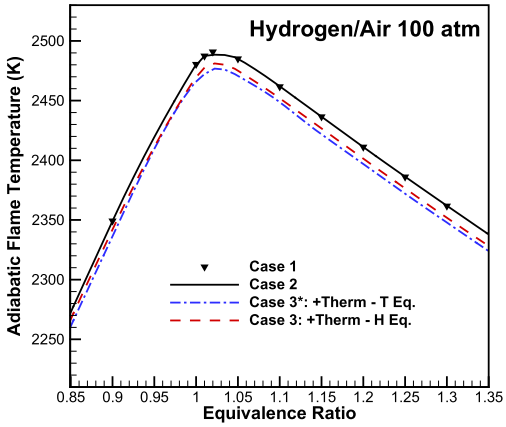

Fig. 5. Adiabatic flame temperature of hydrogen/air at 100 atm for Cases 1–3.

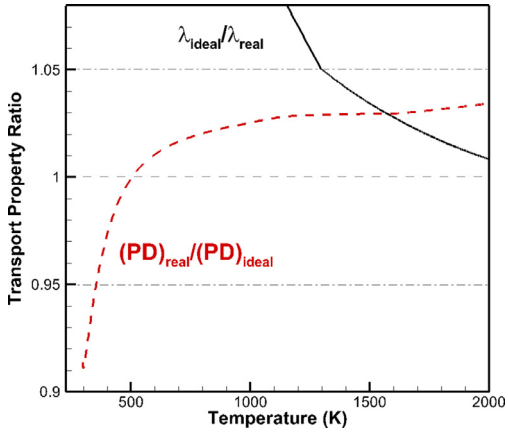

Fig. 6. Transport property ratios of the stoichiometric hydrogen/air flame at 100 atm.

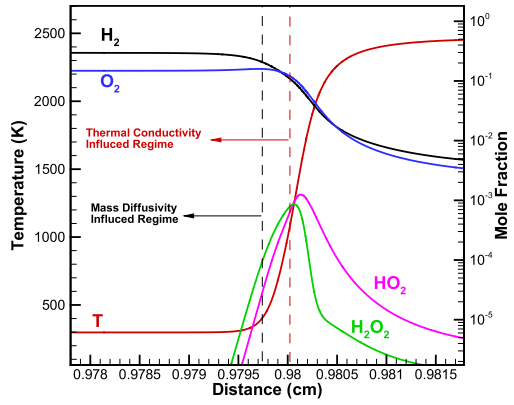

Fig. 7. Transport-affected regimes and flame structure of the stoichiometric hydrogen/air flame at 100 atm.

els. In order to understand this finding, we plot the ratios for these two transport properties, namely thermal conductivity, λ, and the pressure-weighted mass diffusivity, PD, of the ideal gas and real fluid in Fig. 6 with the 5% deviation demonstrated. It is seen that the real-fluid models only have notable influence on the transport properties at relatively low temperatures, which is the condition when the fluid approach the liquid side of the phase diagram. In general, it is reasonable to expect that different descriptions of the transport properties would have much weaker influence on the burning flux, which follows the scaling law [21]: $f \propto \sqrt{(\rho\alpha)w}$, where $(\rho\alpha)$ is a density-weighted diffusivity, and w the global reaction rate. Since $(\rho\alpha)$ is primarily pressure insensitive and only weakly dependent on temperature, then the dependence of the burning flux, and through it the flame speed (for the same density) on the different thermodynamic descriptions through the transport coefficients is correspondingly weak. This in turn implies that the primary dependence of the flame speed is through the change in the global reaction rate w, which is highly sensitive to temperature due to the large activation energy, E_a, through $w \propto \exp(-E_a/RT)$.

Figure 7 shows the temperature and mole fraction profiles of hydrogen and oxygen, as well as the important chain carriers, namely HO_2 and H_2O_2 of the stoichiometric hydrogen/air flame, at 100 atm. The regimes where transport properties have more than 5% deviation with the ideal gas predictions are also indicated. It clearly demonstrates that the transport-affected region is largely decoupled from the reaction region, so they can only influence the preheat zone of the planar flame and do not influence the chemical reactions. This provides an additional reason for the relatively weak influence of the transport properties on the flame propagation rate.

3.2. Planar methane/air flames

Figure 8(a) shows the laminar flame speeds of methane/air mixtures at 100 atm, with different thermodynamic assumptions with the GRI Mech 3.0. It is seen that different from hydrogen/air mixtures, the update of EoS (Cases 1 and 2) has small effect on the flame speed, which implies that the density change of methane/air is not as large as that for hydrogen/air. This is reasonable in that, as shown in Fig. 2, the critical point of methane/air is much higher than that of hydrogen/air, so there is less real-gas compression for the methane/air mixtures. For the effects of thermodynamics and transport (Cases 2–5), the findings are similar to the hydrogen case, which shows that the updated energy equation reduces the flame speed while transport has very small influence.

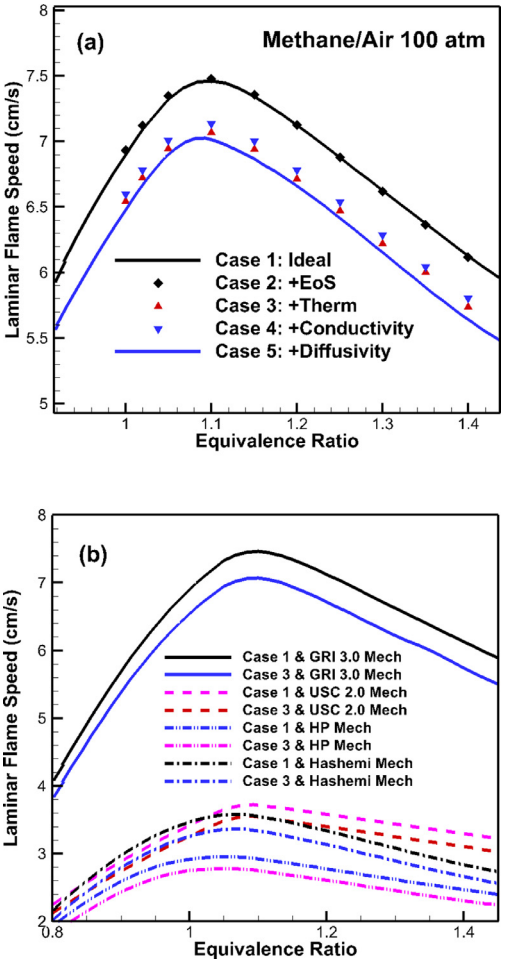

Fig. 8. Laminar flame speeds of methane/air at 100 atm with (a) different assumptions and (b) different kinetic models.

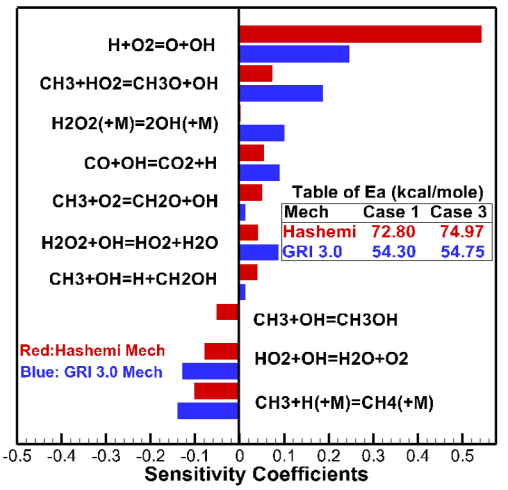

Fig. 9. Sensitivity and global activation energy analysis of stoichiometric methane/air flame at 100 atm.

To assess the effect of chemical kinetic models adopted, the GRI Mech 3.0 [13], the USC Mech 2.0 methane sub-model [14], the HP Mech methane sub-model [15], and the recently updated high-pressure methane sub-mechanism from Hashemi et al. [16] are used to compare with each other, as shown in Fig. 8(b). The HP and Hashemi mechanisms are designed to include more accurate pressure-dependent rates, and have been validated against high-pressure experimental data up to 200 atm. The results show that predictions using the USC 2.0, HP and Hashemi mechanisms, with the flame temperature being either that of Case 1 for the ideal gas or that of Case 3 for the real fluid, are much lower than those using the GRI Mech 3.0. This finding indicates that the accuracy of the kinetic mechanisms used perhaps has the largest sensitivity for such high-pressure applications than the updates of EoS, thermodynamics and transport.

To further identify the cause for the difference with different kinetic models, results from the sensitivity analysis of S_L with the sensitivity coefficient S_i for the ith reaction for Case 3 using GRI 3.0 and the Hashemi mechanisms are compared in Fig. 9. It is seen that the omni-important chain-branching reaction, $H + O_2 = O + OH$, still largely controls the laminar flame speed. Furthermore, the pressure-dependent reactions $CH_3 + H(+M) = CH_4(+M)$ and $H_2O_2(+M) = 2OH(+M)$ are also important, while the termination reaction $CH_3 + OH = CH_3OH$ is missing in the GRI Mech 3.0. These findings indicate that accurate high-pressure rate expressions for these reactions are essential for the correspondingly accurate predictions of the laminar flame speeds. Furthermore, the global activation energies [21], defined as $Ea = -2R[\partial \ln(f)/\partial(1/T_{ad})]$, were calculated and listed in the table in Fig. 9, which shows the sensitivity of the burning flux to variations in T_{ad}. It is then seen that, for the same mechanism, changing from Case 1 to Case 3 has small effect on Ea. However, comparing the two mechanisms, Ea from GRI 3.0 is much lower than that from the Hashemi mechanism. This indicates that such kinetic difference leads GRI 3.0 to predict a much higher value of S_L, as demonstrated in Fig. 8(b).

4. Conclusions

The propagation of hydrogen/air and methane/air flames at supercritical conditions has been simulated for the planar flame configuration. Descriptions of real-gas EoS, thermodynamics, and trans-

port, together with high-pressure chemistry, have been incorporated into the numerical simulations at progressively more complete levels of implementation.

For the laminar flame speed of hydrogen/air mixtures, it is found that it is increased due to the non-ideal equation of state, which is mainly caused by the density modification of the initial mixture. Including the thermodynamic description would reduce the laminar flame speed because of the decreased adiabatic flame temperature through the real-fluid model. Furthermore, the enthalpy format of the energy equation leads to lower laminar flame speed compared with the temperature format of the energy equation. This is because the mixing rule at supercritical state further reduces the mixture enthalpy, hence decreases the flame temperature. Transport models, however, are found to have minimal effect on the laminar flame speed even at very high pressures.

For methane/air flames, the effect of EoS is much weaker than the hydrogen/air flames, which is mainly due to the higher critical points of methane/air mixtures. Furthermore, use of the recently-developed high-pressure kinetics mechanism leads to substantially reduced flame speed at supercritical states; the reason is kinetic in nature in terms of revised rate parameters instead of the different flame temperatures resulting from different supercritical thermodynamic descriptions.

Acknowledgments

This research was sponsored by the US Air Force Office of Scientific Research under the technical monitoring of Dr. Mitat Birkan. WL was in addition supported by a Maeder Fellowship and a Harari Fellowship of Princeton University.

References

[1] A.H. Lefebvre, *Gas Turbine Combustion*, CRC press, 1998.
[2] R.D. Reitz, *Combust. Flame* 160 (2013) 1–8.
[3] G.P. Sutton, O. Biblarz, *Rocket Propulsion Elements*, Wiley & Sons, 1966.
[4] G. Ribert, N. Zong, V. Yang, L. Pons, N. Darabiha, S. Candel, *Combust. Flame* 154 (2008) 319–330.
[5] L. Pons, N. Darabiha, S. Candel, G. Ribert, V. Yang, *Combust. Theory Model.* 13 (2009) 57–81.
[6] H.F. Huo, X.J. Wang, V. Yang, *Combust. Flame* 161 (2014) 3040–3050.
[7] X. Wang, H. Huo, V. Yang, *Combust. Sci. Technol.* 187 (2014) 60–82.
[8] A. Jordà Juanós, W.A. Sirignano, *Combust. Flame* 181 (2017) 54–70.
[9] S. Candel, M. Juniper, G. Singla, P. Scouflaire, C. Rolon, *Combust. Sci. Technol.* 178 (2006) 161–192.
[10] V. Giovangigli, L. Matuszewski, F. Dupoirieux, *Combust. Theory Model.* 15 (2011) 141–182.
[11] R.J. Kee, J.F. Grcar, M.D. Smooke MD, J.A. Miller, E. Meeks, Sandia National Laboratories Report. 1985 (SAND85-8249).
[12] M.P. Burke, M. Chaos, Y. Ju, F.L. Dryer, S.J. Klippenstein, *Int. J. Chem. Kinet.* 44 (2012) 444–474.
[13] G.P. Smith, D.M. Golden, M. Frenklach, et al. GRI 3.0 Mechanism. Gas Research Institute.
[14] H. Wang, X. You, A.V. Joshi, et al., USC Mech Version II. 2007.
[15] H. Zhao, J. Fu, F.M. Haas, Y. Ju, *Combust. Flame* 183 (2017) 253–260.
[16] H. Hashemi, J.M. Christensen, S. Gersen, H. Levinsky, S.J. Klippenstein, P. Glarborg, *Combust. Flame* 172 (2016) 349–364.
[17] G. Soave, *Chem. Eng. Sci.* 27 (1971) 1197–1203.
[18] J.F. Ely, H.J. Hanley, *Ind. Eng. Chem. Fundam.* 22 (1983) 90.
[19] S. Takahashi, *J. Chem. Eng. Jpn.* 31 (1975) 417–420.
[20] P.J. Linstrom, W.G. Mallard, NIST Chemistry webbook, NIST standard reference database No. 69, 2001.
[21] C.K. Law, *Combustion Physics*, Cambridge University Press, 2006.